Supplementary Information

Universal respiration sensing platform utilizing surface water condensation†

Yaodong Guan,[a] Yongming Song,[a] Haoyang Li,[a] Lei Ye,[a] Baoyang Lu,*[b] Jianfeng Zang*[ac] and Yan Yu*[a]

a. School of Optical and Electronic Information, Huazhong University of Science and Technology, 1037 Luoyu Rd., Wuhan, Hubei 430074, PR China
b. School of Pharmacy, Jiangxi Science & Technology Normal University, Nanchang, 330013, Jiangxi, PR China
c. Wuhan National Laboratory for Optoelectronics, Huazhong University of Science and Technology, Wuhan, Hubei 430074, PR China

contents:

1. The supplementary figures: Fig. S1-S6.

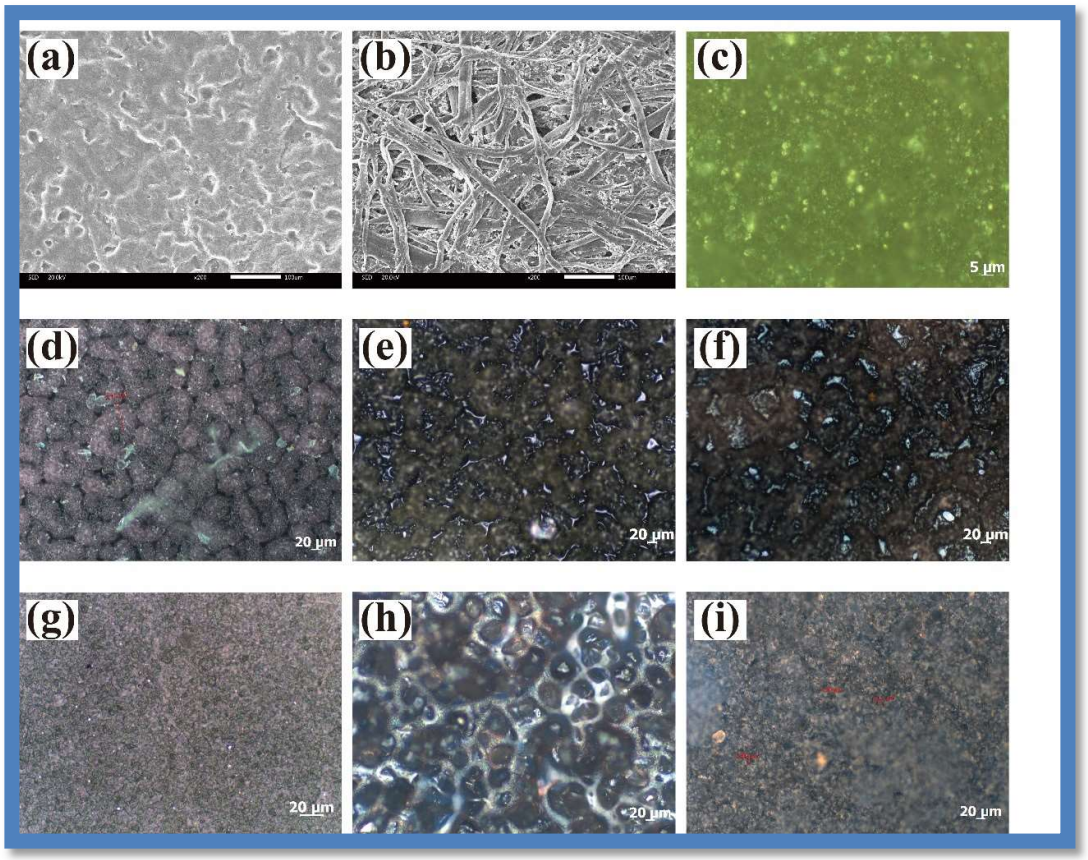

Fig. S1 The surface topography of other suitable sensing materials. (a) The SEM (scanning electron microscope) image of NRF; (b) The SEM image of the cellulose paper; (c-i) The optical microscope images of natural emulsion film, bluelapingcompositefilm (2000 mesh), yellow lappingcompositefilm (1500 mesh), brown lappingcompositefilm (6000 mesh),light green lappingcompositefilm (10000 mesh), granulated abrasive paper (sand paper), stone paper, respectively.

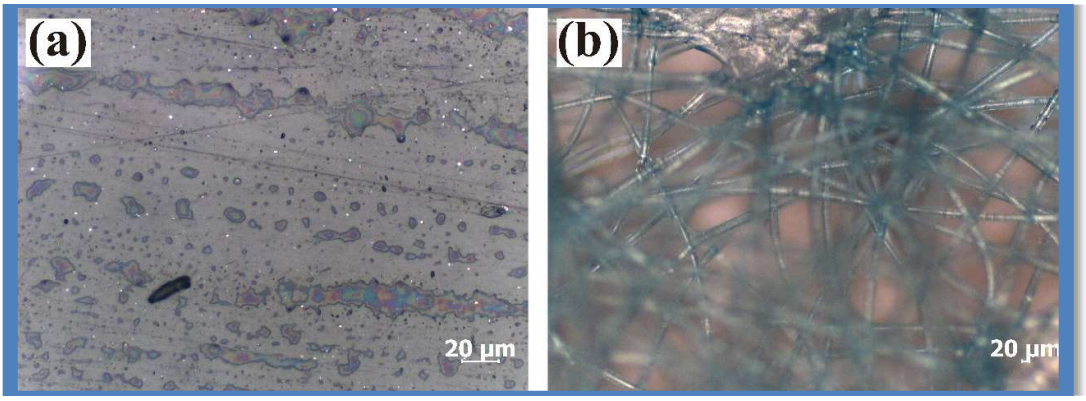

Fig. S2 The surface topography of improper materials. (a) The PE film with extremely smooth surface. (b) Fiber in mask. There are no more hydrophilic groups in these fibers.

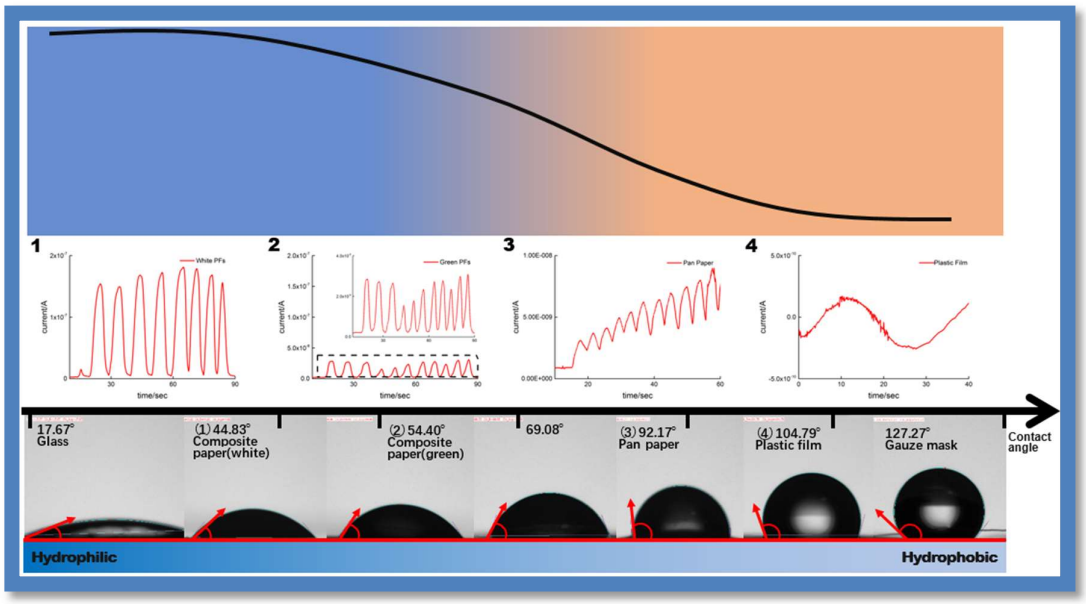

Fig. S3 The surface morphology and contact angle of suitable materials, which shows the relationship between contact angle and condensation. As the contact angle increases, the monitoring signal tends to be bad.

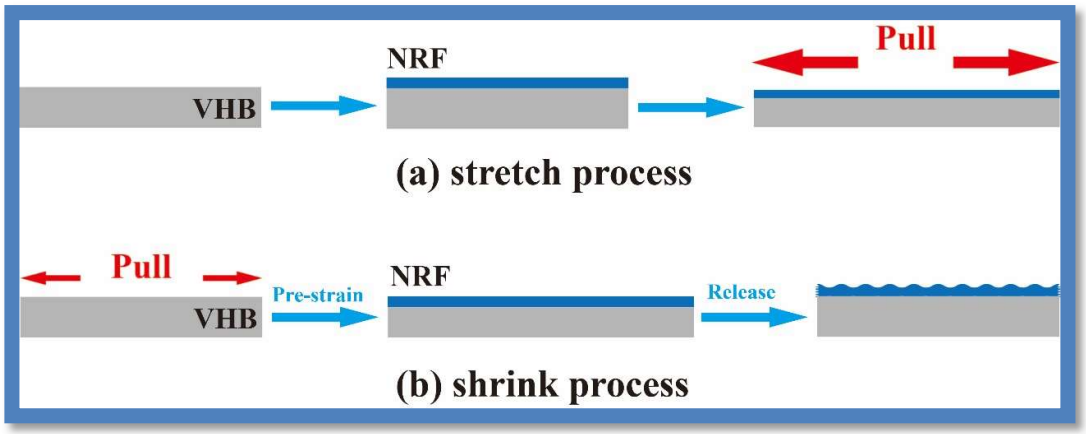

Fig. S4 The preparation process of the stretched sensor and the wrinkled sensor.

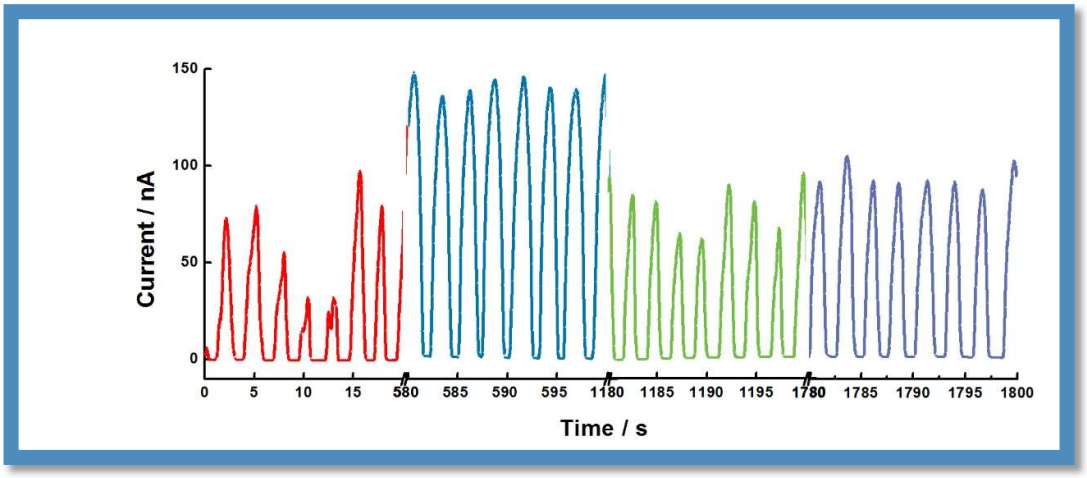

Fig. S5 The monitoring results for continuous monitoring of human respiration over a longer period of 30 minutes. The figure shows the changes in human respiration at different times.

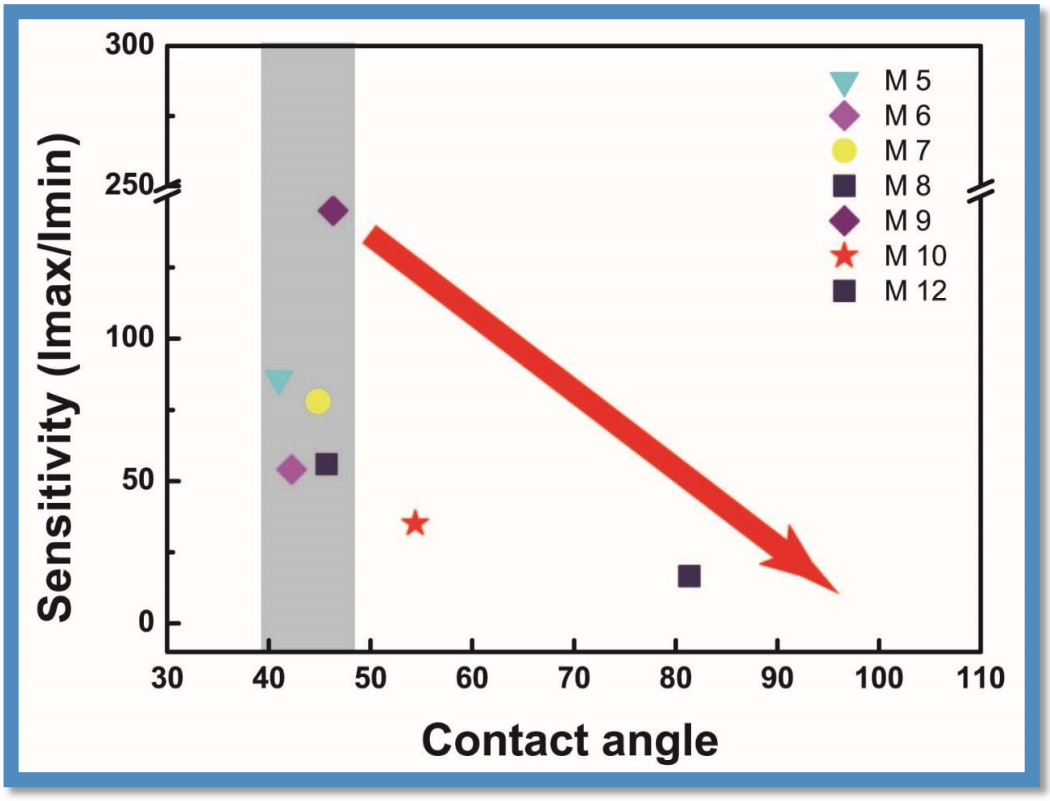

Fig. S6 The relationship between sensor sensitivity and material contact angle, and these materials have the same materials (LCFs) but different surface roughness.

2. Principle supplement: Part 1. The formation of conductive film path based on water condensation mainly for monitoring.

Although dropwise condensation had been realized as early as 1930, the formation mechanism is still controversial. The formation mechanism of the initial droplets has been discussed from different perspective and two hypotheses were raised, called 'the hypothesis of film-rupture' and 'the hypothesis of specific nucleation sites'.[40-42] At present, most of researchers are more supportive of the latter that suggests that nuclei directly initiate at specific nucleation sites, such as pits or cavers.[39,42] We also find that, for materials with suitable roughness as previously given in the literature,[39-46] the droplet nucleation is more likely to occur on surfaces with better trade-off. The granular roughened microstructure surface of selected materials is erose, that can be analogous approximately to the combination of spherical cavities, pits or bulge.

Water condensation is related to many factors of materials, including the surface microtopography, wettability, water contact angle hysteresis and wetting hysteresis.[44] According to the previous researches, it is a common method to use water condensation to approximate the general irregular rough surface with the surfaces which have specific sites, e.g. cavities, pits and cavers, etc.[47]

For the cavities, based on the kinetic theory proposed by Nowakowski and Ruckenstein, Ruckenstein and O. Berim developed a new equation to investigate the effect of cavities radii, contact angle and interaction strength to the nucleation rate in spherical cavities surface on supersaturations.[45] The nucleation rate, I, was provided by the equation

$$\mathrm{I} \cong n_1\beta_1 \frac{S_c(N_*)}{S_c(1)}\left(\frac{H''(N_*)}{2\pi}\right)^{1/2} exp\big(H(N_*)\big). \tag{1}$$

Where n_1 is the number density of the vapor, N_* is the critical cluster size that obtained from Eq. (2), H is the Hamiltonian. The condensation rate, β, is given by Eq. (3), β_1 is one water molecule in the first cluster. The free surface of the cluster which depends on the cluster size, S_c, is obtained from Eq. (4).

$$n_1 = n_w \frac{4\lambda}{\bar{v}} \alpha^1(N_*). \tag{2}$$

Note that the rate of evaporation per molecule, α_1, depends on the cluster size N (number of molecules in the cluster). Where n_w is the number density of the fluid molecules in the well, $\bar{v}$ is the mean velocity of the vapor molecule, λ is the thickness of well.

$$\beta = \frac{\bar{v}}{4} S_c n_1. \tag{3}$$

$$S_c = 2\pi R^2 f_c(x), \tag{4}$$

Where R is the cluster radius, $f_c(x)$ is a geometrical factor and $x = {(R_s - \sigma)}/{R}$. R_s is the radius of the spherical cavities. We can find the following points via the above equations: (1) the lager the curvature, the larger is the nucleation rate (the curvature of plane is zero); (2) the formation of condensation is the most suitable at supersaturations when the cluster has a size comparable with the size of the cavity; (3) the dependence of nucleation rate on the contact angle isn't monotonous both for a cavity and a plane surface.

For pits and cavers, M. Qian and J. Ma analyzed the characteristics of heterogeneous nucleation on concave spherical surface using a novel analytical method.[48] The nucleation on concave spherical surface occur primarily when $2R < 10r_*$ and diminish rapidly when $2R > 10r_*$, while that's the opposite on convex spherical surface (where 2R is the cavity size, $2r_*$ is the nucleus size). That also showed that the nucleation is indeed related to the surface morphology and depends on the roughness of surface or the size of specific sites. According to the idea of differentiation and limit, we think that there is the similar theory on general irregular rough surface, that is positive correlation between the nucleation and the roughness of surface. Our speculation can be verified by the previous study. Tianqing Liu, etc. studied the relationship of nucleation site density with surface topography for dropwise condensation.[44] Fractal dimension, D, was used to describe the irregularity and complexity of a rough surface and measured by the differential box-counting method.[46] The rougher a surface the larger the fractal dimension. The nucleation site density, N_s, can be expressed as follows:

$$N_s = \frac{0.01+2.019\times10^{-2}\ e^{15.62D}}{r_{min}^2}. \quad (5)$$

Where r_{min} is the minimum nuclear radius. They found that the probability of generating more active sites increases as the higher fractal dimension of the condensation surface reveals more flaws such as pits, sidelines and edges on the surface. These active sites are conductive to forming initial nuclei. That is, the rougher a surface, the more the nucleation sites on it.[44] In addition, dropwise condensation is related to other factors, including wettability, water contact angle hysteresis and wetting hysteresis. Therefore, in order to achieve high-performance monitoring for human respiration, the sensing materials with high-roughness and proper-fluctuation need to be selected.

3. Measurement method of average sensitivity and fastest response/recovery time of each sensor.

Current: We determined that the current before the start of the first breath is the baseline current, as shown in the blue box in the figure. This baseline current takes into account of effects of ambient humidity and instrument noise. The Imax (Imin) for each material is the average of the peak of 50 breath cycles. Changes caused by environmental disturbances and instrument noise are negligible compared to lager current

peaks.

Time: Changes in ambient temperature and humidity, instrument noise, and human respiratory airflow conditions all have impact on response time and recovery time. The definition of response/recovery time is already stated in the "*measurement parameter*" section. The data in the figure is the average of the results after 50 independent tests.

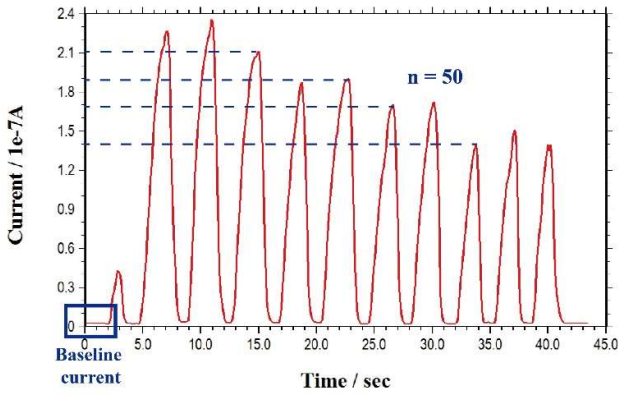

4. The supplementary tables: Table S1-S2.

Table S1. Comparison of Humidity Sensing Performance of Humidity (respiration) Sensors in Recent Literature.

Sensing Materials	Time (s)		Sensitivity	Applied Voltage (V)	Refs.
	Response	Recovery			
Cellolose paper	1500	N/A	<10	25	Whitesides et al.[13]
Henzocyclobutene	216	N/A	~30	11 (max)	Zampetti et al.[53]
Hydrophilic polytetrafluoroethylene membrane	1	1	N/A	N/A	Miyoshi et al.[54]
SnO_2 nanowire	120-170	20-60	32	1	Kuang et al.[55]
LiCl doped TiO_2 nanofibers	3	6	23	N/A	Zhang et al.[56]

Graphene oxide / polyelectrolyte nanocomposite	1	1	10^3	N/A	Zhang et al.[57]
Silicon-nanocrystal film	0.04	0.04	10^5	5	Fujii et al.[58]
Carbon nanoparti-cle “skin”	N/A	N/A	~55	N/A	Zhang et al.[59]
Black phosphorus flakes	60	30	10^4	0.5	Salehi-Khojin et al.[60]
Nafion per-fluorosulfonate	0.04	0.03	500	5	Dasgupta et al.[61]
ABTS and $C_{10}(mim)_2$	0.037	~ 0.1	N/A	0.5	Mao et al[62]
Supramolecular nanofiber	2.2	1.05	10^4	0.8	Kulkarni et al.[63]
Graphene oxide	0.03	0.03	N/A	N/A	Tapani et al.[64]
Polyaniline-PVA composites film	45	540	10^3	N/A	Shiigi et al.[65]
WS_2 film	~1	~ 1	<5	<10	Li et al.[66]
CNTs and NWF	N/A	N/A	<10	N/A	Donghe Du et al.[67]
SWCNT/PVA fil-aments	40	N/A	24	N/A	Chou et al.[68]
SiC nanopaper	0.8	5.6	~10	N/A	Li et al.[69]
WS_2	~12	~13	~137	N/A	Sandesh et al.[70]
activated alumina powder	10	600	N/A	N/A	Sotiris et al.[71]
Silk fabrics and GO	N/A	N/A	$\sim 10^2$	1	Bintian Li et al.[72]
Polyimide (PI)/paper bilayer	~22 times per minute	N/A	<10	N/A	Jiangjiang Luo et al.[73]
NRF	**0.19**	**0.8**	**10^3**	**1**	**This work**

Table S2. Contact angle and microscope Images of materials with the same materials (LCFs) but with different surface roughness.

Various LCFs	Contact Angle Images	Microscope Images
M5: Blue LCF (2000 mesh) 41.01°		
M6: Yellow LCF (1500 mesh) 42.24°	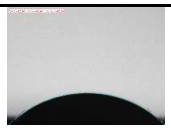	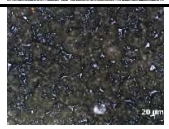
M7: White LCF (12000 mesh) 44.83°		
M8: Brown LCF (6000 mesh) 45.68°		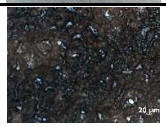
M9: Pink LCF (8000 mesh) 46.31°	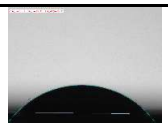	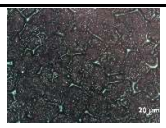
M10: Green LCF (800 mesh) 54.40°		
M12: Light green LCF (10000 mesh) 81.58°		

References

13 F. Güder, A. Ainla, J. Redston, B. Mosadegh, A. Glavan, T. J. Martin and G. M. Whitesides, *Angew. Chemie - Int. Ed.*, 2016, **55**, 5727–5732.

39 I. O. Ucar and H. Y. Erbil, *Appl. Surf. Sci.*, 2012, **259**, 515–523.

40 J. W. Rose, *Proc. Inst. Mech. Eng. Part A J. Power Energy*, 2002, **216**, 115–128.

41 Y. Utaka and N. Terachi, *Trans. Japan Soc. Mech. Eng. Ser. B*, 1995, **61**, 1063–1069.

42 L. Tianqing, M. Chunfeng, S. Xiangyu and X. Songbai, *AIChE J.*, 2006, **53**, 1050–1055.

43 I. Orkan Uçar and H. Y. Erbil, *Turkish J. Chem.*, 2013, **37**, 643–674.

44 C. Mu, J. Pang, Q. Lu and T. Liu, *Chem. Eng. Sci.*, 2008, **63**, 874–880.

45 E. Ruckenstein and G. O. Berim, *J. Colloid Interface Sci.*, 2010, **351**, 277–282.

46 Y. T. Wu, C. X. Yang and X. G. Yuan, *Int. J. Heat Mass Transf.*, 2001, **44**, 4455–4464.

47 F. Rosei, *J. Phys. Condens. Matter*, 2004, **16**, S1373.

48 M. Qian and J. Ma, *J. Cryst. Growth*, 2012, **355**, 73–77.

53 E. Zampetti, S. Pantalei, A. Pecora, A. Valletta, L. Maiolo, A. Minotti, A. Macagnano, G. Fortunato and A. Bearzotti, *Sensors Actuators B Chem.*, 2009, **143**, 302–307.

54 Y. Miyoshi, K. Miyajima, H. Saito, H. Kudo, T. Takeuchi, I. Karube and K. Mitsubayashi, *Sensors Actuators B Chem.*, 2009, **142**, 28–32.
55 Q. Kuang, C. Lao, Z. L. Wang, Z. Xie and L. Zheng, *J. Am. Chem. Soc.*, 2007, **129**, 6070–6071.
56 Z. Li, H. Zhang, W. Zheng, W. Wang, H. Huang, C. Wang, A. G. MacDiarmid and Y. Wei, *J. Am. Chem. Soc.*, 2008, **130**, 5036–5037.
57 D. Zhang, J. Tong, B. Xia and Q. Xue, *Sensors Actuators B Chem.*, 2014, **203**, 263–270.
58 S. Kano, K. Kim and M. Fujii, *ACS Sensors*, 2017, **2**, 828–833.
59 Y. Deng, J. Liu, E. Mäder, G. Heinrich, J. Zhang and S. Gao, *Adv. Mater. Interfaces*, 2015, **2**, 1–6.
60 P. Yasaei, A. Behranginia, T. Foroozan, M. Asadi, K. Kim, F. Khalili-Araghi and A. Salehi-Khojin, *ACS Nano*, 2015, **9**, 9898–9905.
61 P. Kuban, J. M. Berg and P. K. Dasgupta, *Anal. Chem.*, 2004, **76**, 2561–2567.
62 H. Yan, L. Zhang, P. Yu and L. Mao, *Anal. Chem.*, 2017, **89**, 996–1001.
63 U. Mogera, A. A. Sagade, S. J. George and G. U. Kulkarni, *Sci. Rep.*, 2014, **4**, 1–9.
64 S. Borini, R. White, D. Wei, M. Astley, S. Haque, E. Spigone, N. Harris, J. Kivioja and T. Ryhänen, *ACS Nano*, 2013, **7**, 11166–11173.
65 K. Ogura, T. Saino, M. Nakayama and H. Shiigi, 1997, **7**, 2363–2366.
66 H. Guo, C. Lan, Z. Zhou, P. Sun, D. Wei and C. Li, *Nanoscale*, 2017, **9**, 6246–6253.
67 D. Du, Z. Tang and J. Ouyang, *J. Mater. Chem. C*, 2018, **6**, 883–889.
68 G. Zhou, J. H. Byun, Y. Oh, B. M. Jung, H. J. Cha, D. G. Seong, M. K. Um, S. Hyun and T. W. Chou, *ACS Appl. Mater. Interfaces*, 2017, **9**, 4788–4797.
69 G. Y. Li, J. Ma, G. Peng, W. Chen, Z. Y. Chu, Y. H. Li, T. J. Hu and X. D. Li, *ACS Appl. Mater. Interfaces*, 2014, **6**, 22673–22679.
70 A. S. Pawbake, R. G. Waykar, D. J. Late and S. R. Jadkar, *ACS Appl. Mater. Interfaces*, 2016, **8**, 3359–3365.
71 J. Van Den Broek, A. T. Güntner and S. E. Pratsinis, *ACS Sensors*, 2018, **3**, 677–683.
72 B. Li, G. Xiao, F. Liu, Y. Qiao, C. M. Li and Z. Lu, *J. Mater. Chem. C*, 2018, **6**, 4549–4554.
73 J. Luo, Y. Yao, X. Duan and T. Liu, *J. Mater. Chem. C*, 2018, **6**, 4727–4736.